Comparison of Geosynchronous Satellites Spectral Signatures During Glint Season

Daniel E. Weisz and Francis K. Chun
Department of Physics, U.S. Air Force Academy

ABSTRACT

Cadets in the Department of Physics at the United States Air Force Academy are using the technique of slitless spectroscopy to analyze the spectra from geostationary satellites during glint season. The equinox periods of the year are particularly favorable for earth-based observers to detect specular reflections off satellites (glints), which have been observed in the past using broadband photometry techniques. Three seasons of glints were observed and analyzed for multiple satellites, as measured across the visible spectrum using a diffraction grating on the Academy's 16-inch, f/8.2 telescope. It is clear from the results that the glint maximum wavelength decreases relative to the time periods before and after the glint, and that the spectral reflectance during the glint is less like a blackbody. These results are consistent with the presumption that solar panels are the predominant source of specular reflection. The glint spectra are also quantitatively compared to different blackbody curves and the solar spectrum by means of absolute differences and standard deviations. Our initial analysis appears to indicate a potential method of determining relative power capacity.

1. INTRODUCTION

Man-made satellites serve a variety of purposes from navigation to remote sensing. Geostationary orbits are among the most important types of orbits in that satellites can orbit the earth at a rate which matches the speed of the rotation of the earth, in effect causing these satellites to appear fixed above the same point on earth. Approximately 400 geostationary satellites (GEOs) facilitate communications, weather forecasting, and security operations around the globe. Although many GEO satellites are large, they are too far away to obtain a high-resolution image by any current ground-based optical telescope. However, using unresolved optical measurements such as spectroscopy, the satellites can be characterized and discriminated. Spectral measurements can be used to attempt to find patterns and irregularities with the satellites, which can enhance our space situational awareness (SSA) of the space environment by identifying changes to normal behavior or appearance.

To characterize the optical features of satellites, the sunlight reflected off of them has been observed in a variety of means, from broadband photometry to spectroscopy [1-6]. Across the visible spectrum certain wavelengths have greater intensities than others, but to first order reflections look very much like the solar spectrum. Researchers can take this data and discern a number of satellite features, such as the composition of the satellite based on the relative intensities in different sections of the spectra or satellite solar panel orientation.

Spectral measurements using a diffraction grating are not new to the community [4, 5]. Hoag and Schroeder developed rudimentary slitless spectroscopic techniques in 1970 [7]. More recently, cadets at the United States Air Force Academy (USAFA), as a part of their senior capstone course in the physics major, have developed and refined the procedures for taking and calibrating satellite spectral measurements [8]. The goal of this research is to measure the optical signature of a GEO satellite under a certain illumination condition favorable to glints. Previously, observations of glints using multi-color, broadband photometry show a characteristic peak in intensity around the zero phase angle [9], however, there has only recently been any observations of glints made via slitless spectroscopy techniques [10]. This paper discusses satellite glints and their cause, presents the instrumentation and collection procedures, shows observational spectra for six GEO satellites, and compares those spectra to a blackbody spectrum.

2. SATELLITE GLINTS

Glints are a unique opportunity to observe optical signatures that can perhaps give insight into the composition, size and orientation of the solar panels on each of the geosynchronous satellites [11]. A glint is a specular or mirror-like reflection due to a unique geometry when the phase angle bisector (i.e. the bisector of the solar phase angle formed by the vector between the satellite and the sun and the satellite and the earth observer) comes close to the normal of a satellite facet. Although this condition can occur at any time, for an earth-bound observer, this condition usually

occurs around the two equinox periods when the orbital inclination of a 3-axis stabilized GEO satellite approaches that of the ecliptic plane. For this research, we observed the glints that occurred around the vernal equinox for five GEO satellites, all of which are U.S. communications satellites with large deployable solar panels. Fig. 1 shows an artist rendition of two of the satellites.

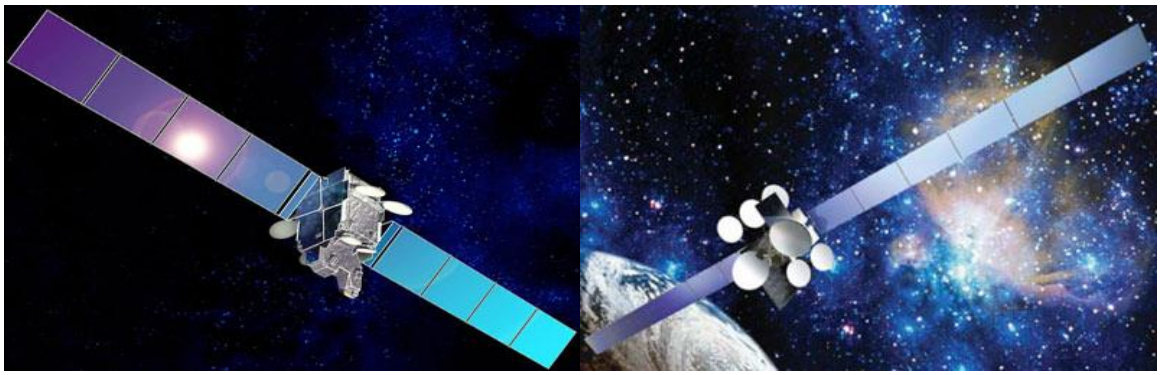

Fig. 1. Artist rendition of Wildblue-1 (left) and DirecTV-12 (right). Images taken from Gunter's Space Page (http://space.skyrocket.de/).

Normally, when the phase angle is not optimal for glinting, the sunlight reflected off the satellite is predominantly diffusive, dispersing in all directions, and the reflected light that reaches the ground observer may display distinct spectral features of the material off which it was reflected [12]. In contrast, reflected specular light should be similar to the source spectrum [12]. However, when a satellite glints, the resulting spectra can perhaps include spectral characteristics of the material off of which it reflects. For instance, satellite solar panels are designed to absorb much of the visual spectrum, especially the red part which contains most of the solar energy flux, thus we surmise that during a glint, more light would be reflected from the blue end of the solar spectrum. Additionally, if a satellite glint is primarily due to specular reflection off of the solar panels, the occurrence of a glint relative to solar phase angle or even the number of glints can provide insight as to how a satellite owner orients their solar panels relative to each other and to the sun.

3. INSTRUMENTATION AND PROCESSING

We collected data using a DFM Engineering f/8.2, 16-inch Ritchey-Chrétien telescope at the USAFA Observatory (Fig. 2). It is outfitted with an Apogee U47 CCD camera that has a 1024×1024 size focal plane with 13μm pixels, providing a field of view of 0.23 degrees or approximately 13 arc minutes on a side. In front of the camera is a nine-position filter wheel which has a 100 lines per millimeter diffraction grating in one of the slots. The theoretical resolution of our diffraction grating is $103 < R < 147$ for a wavelength range of $350 \text{ nm} < \lambda < 700 \text{ nm}$ [13].

Sample images of two GEO satellites is shown in Fig. 3 below which shows Wildblue-1 and Anik-F2 in the left panel image, and Spaceway-1, DirecTV-10, and DirecTV-12 in the right panel image. Both images are of a seven-second exposure. The zero-order of the diffraction pattern is clearly seen toward the top of the image, while the corresponding first-order diffraction spectrum is seen below its zero-order. One can also see star trails and sometimes their corresponding spectra throughout the image which can occasionally corrupt the satellite spectra. The density of the stellar background at magnitudes equal or brighter than the subject satellite will drive the maximum exposure period for the satellite. For instance, the average mean free path of a GEO satellite with magnitude 17 is of the order of ten seconds [4]. Fortunately, because our subject satellites are relatively bright (magnitude < 12), the camera exposure period is usually less than ten seconds thus lowering the probability of star corruption. However, care must be exercised to ensure that we eliminate any image that appears to show this situation.

Fig. 2. USAF Academy's 16-inch telescope used for this research.

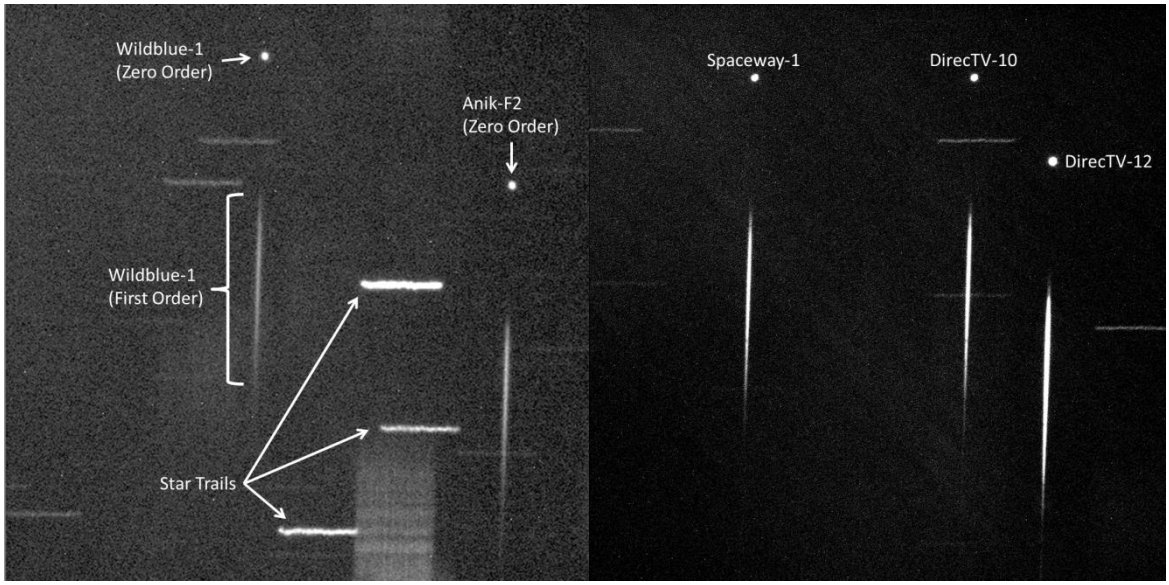

Fig. 3. Example raw images of spectra taken with the USAFA 16-inch telescope. The left panel shows the two GEO satellites Wildblue-1 and Anik-F2 while the right panel shows the GEO cluster of Spaceway-1, DirecTV-10, and DirecTV-12.

The data reduction process we used is outlined in Fig. 4 below, portions of which were developed over the past few years by three different USAFA cadet teams as part of their senior physics capstone research project [8]. The raw data from the telescope CCD (e.g. Fig. 3) is processed through several refinement and reduction steps before we can start to analyze the results. The first step in the data reduction is to rotate the raw image data due to a small misalignment of the diffraction grating relative to the camera's focal plane resulting in a slight angle in the diffraction pattern relative to a vertical reference line in the image. The rotated image can be seen in Fig. 5. We then find the center of the zeroth order spectrum, and clip the image to create a sub-image consisting of a narrow column ranging from 15 to 20 pixels wide centered on the first order diffraction pattern. We then correct for the bias and thermal noise in the CCD camera. Because this paper examines the relative nature of a satellite's spectra before, during and after a glint, we can forgo removing solar features as well as conducting an absolute calibration.

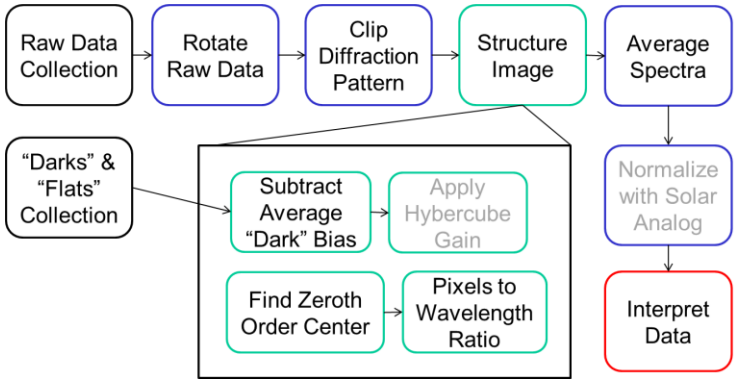

Fig. 4. Data Reduction process used for this research project.

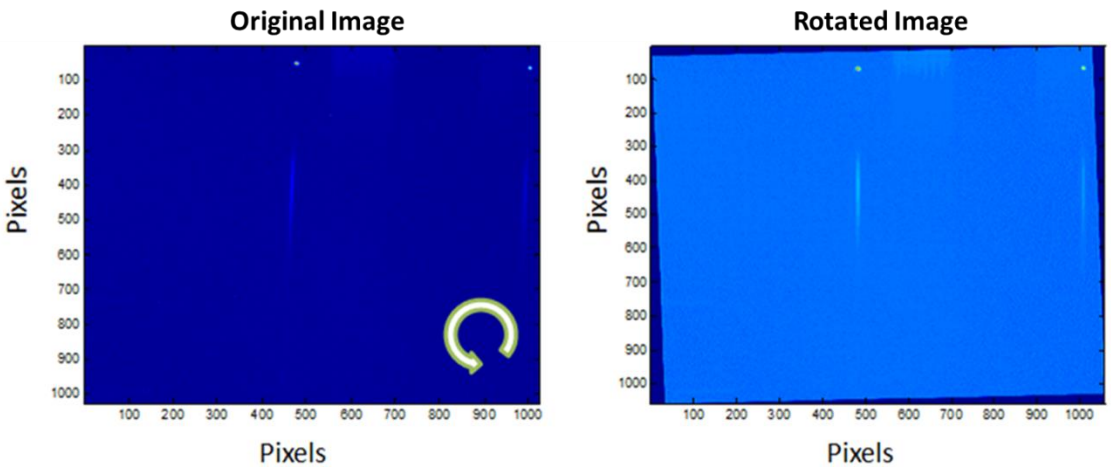

Fig. 5. Rotation of the image due to misalignment of the diffraction grating to camera's focal plane.

The arrays of clipped intensities are in units of pixels versus counts, so in order to investigate the wavelength dependencies in the spectra, we must convert the spectra from pixel space to wavelength space. To do so, we can use emission lines of Wolf-Rayet stars or absorption lines of calibration stars to determine the pixel-to-wavelength conversion for this telescope-camera system. This was accomplished previously by other cadet teams, so since there have not been any changes to our telescope-camera system, we can use their results [8]. The pixel-to-wavelength conversion is given by:

$$\lambda = 1.646P + 5.752 \tag{1}$$

where λ is the calibrated wavelength and P is the distance from the zeroth order in pixels. The result of applying this conversion can be seen in Fig. 6.

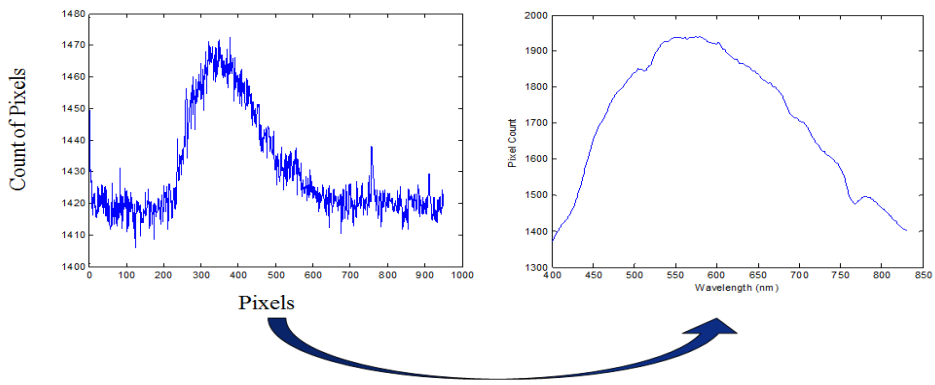

Fig. 6. Conversion of spectra from pixel space to wavelength space. The left panel is a single spectra while the right panel shows a spectra averaged from ~10 individual spectra.

4. RESULTS

We were able to collect data from multiple satellites during three glint seasons, some of which unfortunately do not exhibit any glints. A summary of the glints we were able to observe, including satellite bus information, can be found in Table 1. Fig. 7 shows a time series of spectra for one of these satellites, Wildblue-1 taken the night of 23 February 2015. For a relative comparison of the satellite spectra through the night, the z-axis is in counts per second, the x-axis is wavelength in nanometers, and the y-axis is time in seconds from the first image. One can easily see a dramatic increase in the spectra starting around the 2,000-seconds mark. This is a clear glint off the satellite, and its spectra to first order looks dramatically different prior to and after the glint.

Table 1. Summary of Data Collection. Only observations which included glints are shown. Power Consumption is approximate and based on satellite bus specifications.

Satellite	**Dates of Observations**	**Satellite Bus**	**End-of-Life Power**
Anik-F2	20 October 2016	Boeing BSS-702	15 kW
DirecTV-10	24 October 2015 18 October 2016	Boeing BSS-702HP	12 kW
DirecTV-12	7 March 2015	Boeing BSS-702HP	12 kW
WildBlue-1	23 February 2015 9 March 2016	SSL LS-1300	5 kW
AMC-15	9 October 2015 16 March 2016	Lockheed A2100AXS	4 kW
AMC-18	9 October 2015	Lockheed A2100A	4 kW

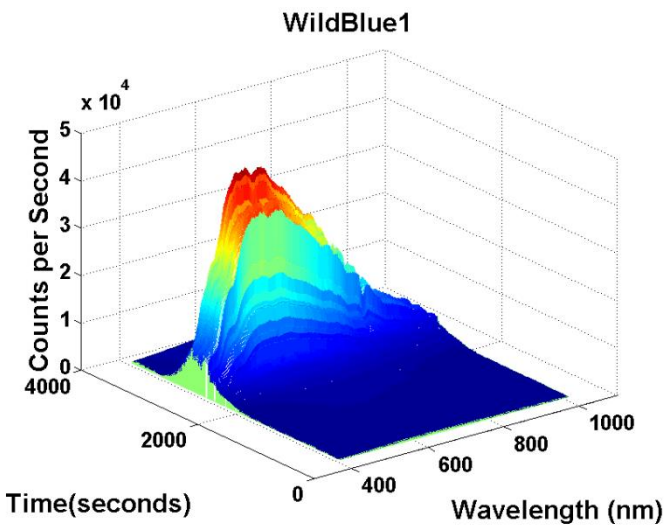

Fig. 7. Processed spectra for Wildblue-1 showing the increase in the count per second as a function of wavelength and time.

For instance, Fig. 8 shows the average of 150 Wildblue-1 spectra taken (a) before, (b) during, and (c) after the glint. The spectra before a glint (Fig. 8a) shows the peak of curve to be >550 nanometers as indicated by the leftmost arrow in the plot. During the glint (Fig. 8b), we noticed that the peak shifted toward the blue end of the visible spectra to about 500 nanometers, and after the glint (Fig. 8c) the peak of the average spectra returned back to >550 nanometers. This appears to support our intuition that the main glint of a stable GEO satellite is caused primarily by its solar panels. Solar panels are designed to absorb solar flux, so it follows that since the majority of the solar energy is toward the red to near infrared end of the solar spectrum, a measured increase in a satellite's reflectance (i.e. a glint) would be toward the blue end. As a reference point to ensure there is no systematic bias in our spectra, the Fraunhofer O_2 absorption line (~760 nanometers) is used to maintain consistency between the averages. For all three averages this trough is around 765 nanometers, which is within the resolution of our diffraction grating measurements.

We also note that all three plots are from 350-850 nanometers in the x-axis, while the y-axis for the middle plot of the glint spectra (b) is 4x larger than the other two plots (a and c). To first order, the glint spectrum (b) has a very different profile compared to the non-glint spectra, as the slope on both the blue end and red end of the glint spectrum is much steeper than the comparable non-glint spectra. We will present further analysis of the spectra later in this paper in regards to how they compare to a blackbody curve.

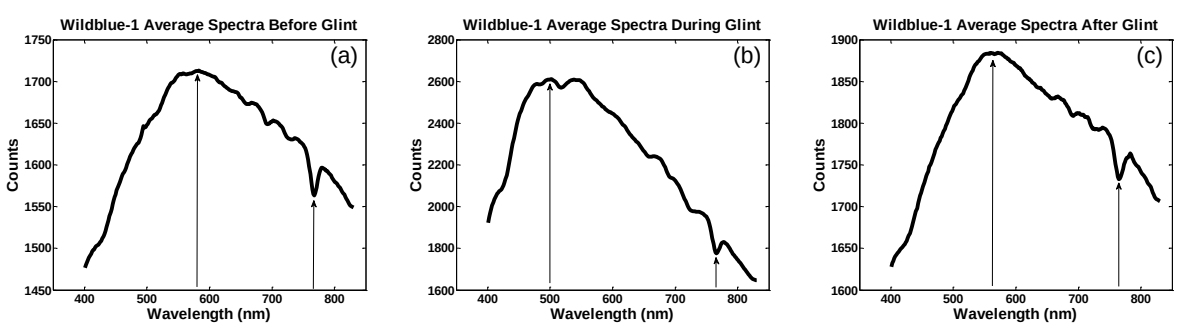

Fig. 8. Average spectra for Wildblue-1 (a) before a glint, (b) during a glint, and (c) after a glint.

Figs. 9-17 below shows the spectral plots for each individual satellites. These plots are similar to the format of the plots seen in Fig. 7 except now seen from above the z axis. The color shows relative intensity with blue being on the lower end and red being higher values. The glint can be very easily identified as the sudden increase in intensity. The black trace superimposed over the mesh shows the wavelength in each spectrum where the max counts per

second occurs. Several characteristics stand out in the individual satellite spectra. Two satellites exhibit two distinct glints, DirecTV-12 (Fig. 13) and AMC-18 (Fig. 16), whereas the other satellites only have a single glint. AMC-15's glint exceeds 10^5 counts per second (Fig. 14) while others are more in the range of 10^4 counts per second (Fig. 9, 11, 12, 13, 16). Another interesting feature seen in three of the satellite glint spectra (Fig. 11, 12, 14, 16) are the presence of a strong bright feature around 600-700 nm. This feature will be seen more clearly in the blackbody analysis and comparison section.

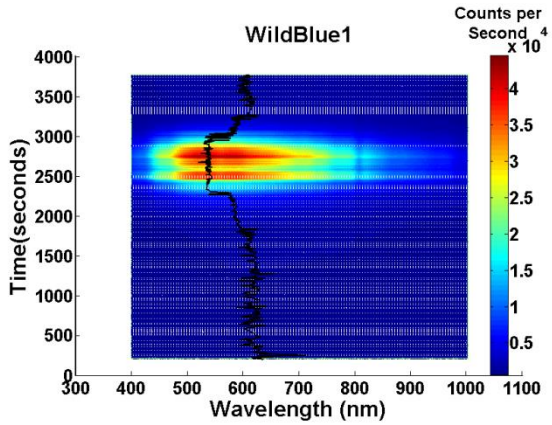

Fig. 9. Individual satellite spectra for Wildblue-1 as observed on 23 February 2015. The x-axis is wavelength, the y-axis is time in seconds from the start of the data collection, and the z-axis is in counts per second.

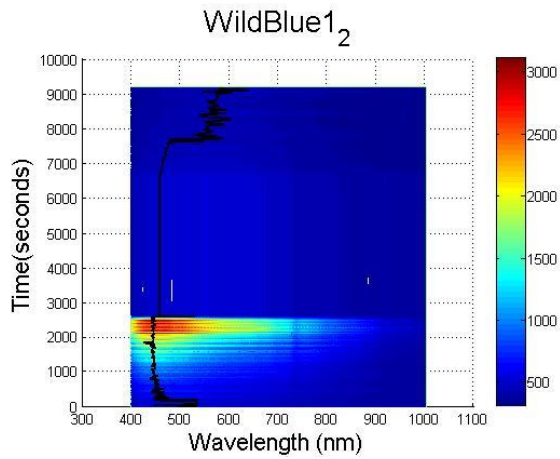

Fig. 10. Individual spectra for WildBlue-1 as observed on 9 March 2016 (same format as Fig. 9).

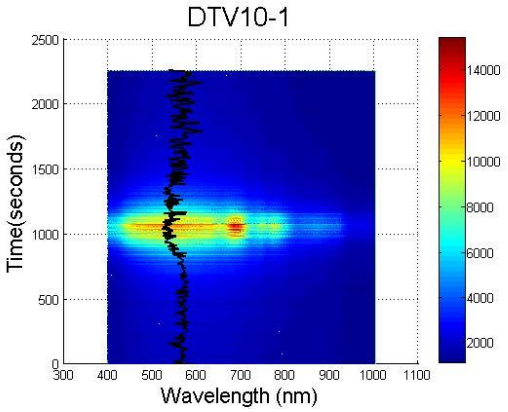

Fig. 11. Individual spectra for DirecTV-10 as observed on 24 October 2015 (same format as Fig. 9). Note: this data represents the first ~2300 seconds of data collection for this night; the last ~2400 seconds were clipped for clarity.

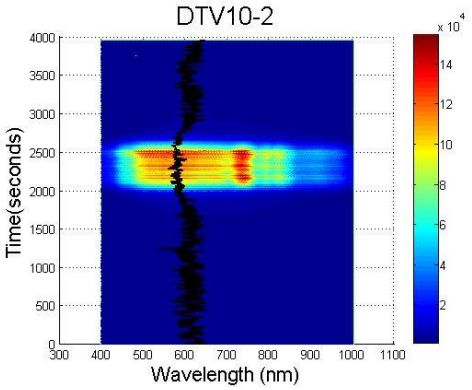

Fig. 12. Individual spectra for DirecTV-10 as observed on 18 October 2016 (same format as Fig. 9). Note: this data starts ~3000 seconds after data collection started for this night; the rest of the data were clipped for clarity.

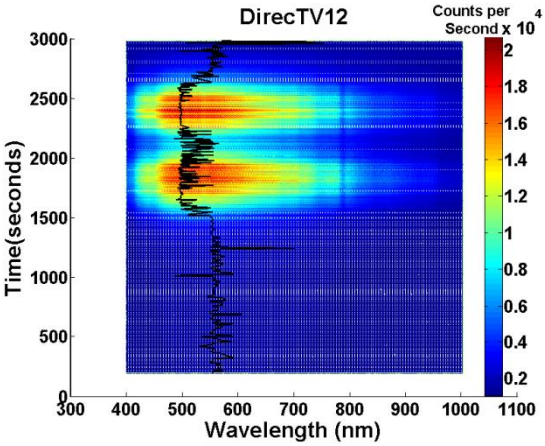

Fig. 13. Individual spectra for DirecTV-12 as observed on 7 March 2015 (same format as Fig. 9).

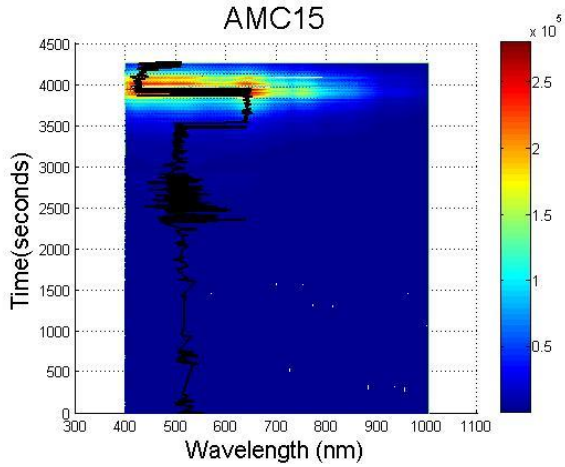

Fig. 14. Individual spectra for AMC15 as observed on 9 October 2015 (same format as Fig. 9).

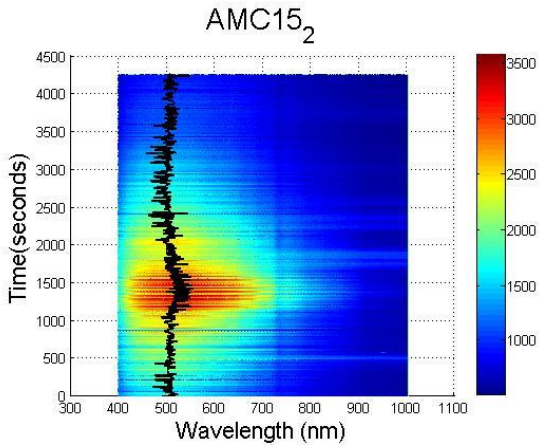

Fig. 15. Individual spectra for AMC15 as observed on 16 March 2016 (same format as Fig. 9).

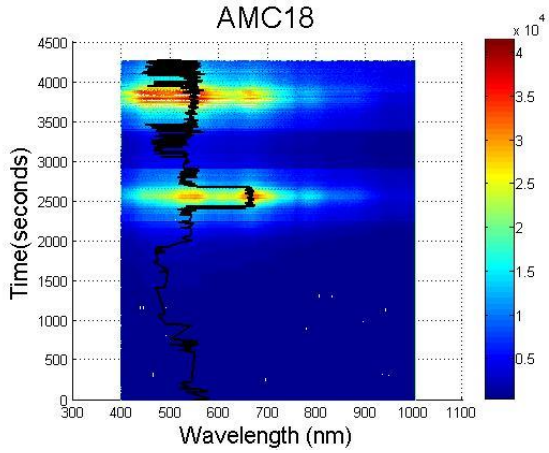

Fig. 16. Individual spectra for AMC18 as observed on 9 October 2015 (same format as Fig. 9).

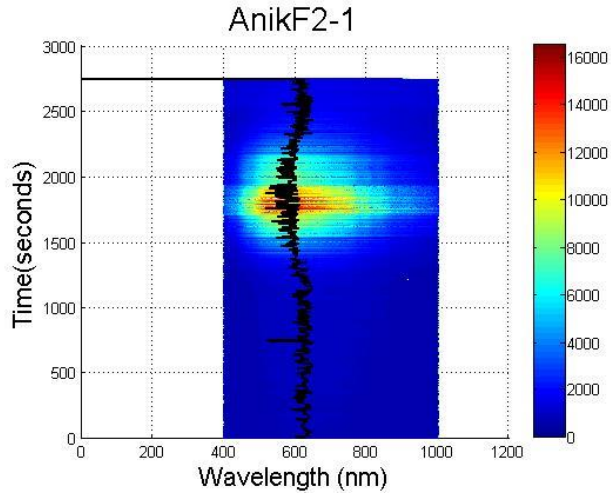

Fig. 17. Individual spectra for Anik-F2 as observed on 20 October 2016 (same format as Fig. 9). This data represents the last ~2800 seconds of data collection for the night; the first ~6500 seconds were clipped for clarity.

5. BLACKBODY COMPARISON

Since a satellite's optical signature as measured by a ground-based telescope is dominated by solar reflectance, we conducted a comparison of the measured satellite spectra to a blackbody spectrum. The satellite reflectance is usually modeled as a combination of diffuse and specular components which can be from a number of major subsystems such as the spacecraft bus and solar panels [9, 12, 14]. Regardless of whether it is diffusive or specular, if there is no absorption of photons by the satellite, then the measured reflectance spectra - especially the specular reflectance - should mimic to first order that of the solar spectrum. If however the premise is true that a satellite glint is primarily due to specular reflection off the solar panel, then we would expect the satellite reflectance spectra to be less like a blackbody due to absorption of solar photons by the solar panels. Figs. 18-23 show the average satellite spectra (black trace) (a) prior to, (b) during, and (c) after the glint for some of the observed satellites. The averages before and after the glint period were taken only from spectra where their maxima was less than 15% of the glint maximum, whereas the average during the glint period was from spectra that had maxima greater than 85% of the glint maximum. Additionally, because the pixel-to-wavelength conversion gives us spectra at 1.646 nm steps, we applied a three-point running average to smooth the data to better reflect the theoretical wavelength resolution of the diffraction grating.

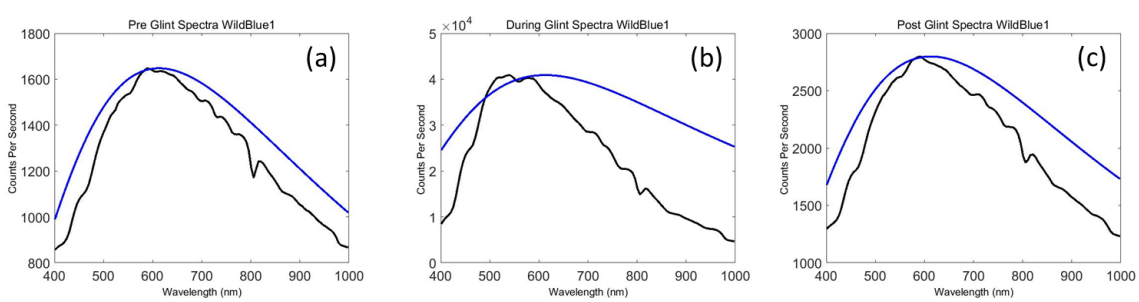

Fig. 18. WildBlue-1 average spectra (a) pre-glint, (b) during glint, and (c) post-glint as observed on 23 Feb 2015. The blue trace indicates blackbody reflectance spectrum for a 4,747K object and the black trace indicates the data.

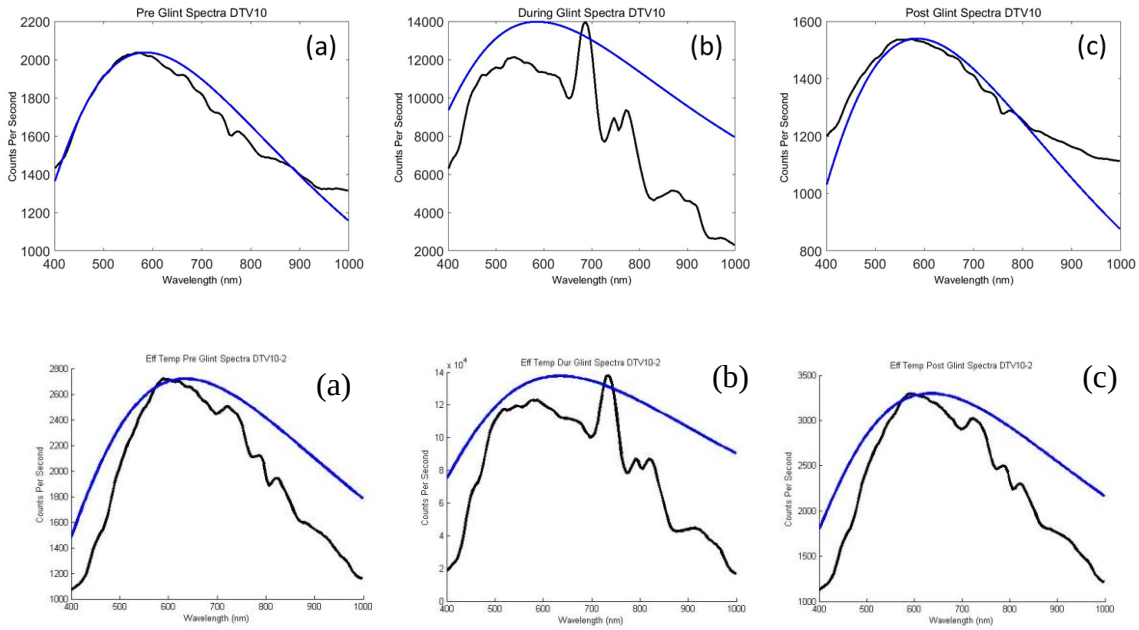

Fig. 19. DirecTV-10 average spectra (a) pre-glint, (b) during glint, and (c) post-glint. The top row is from the first observation, and the second row is from the second observation. The blue trace indicates blackbody reflectance spectrum for a 4,945K object and the black trace indicates the data.

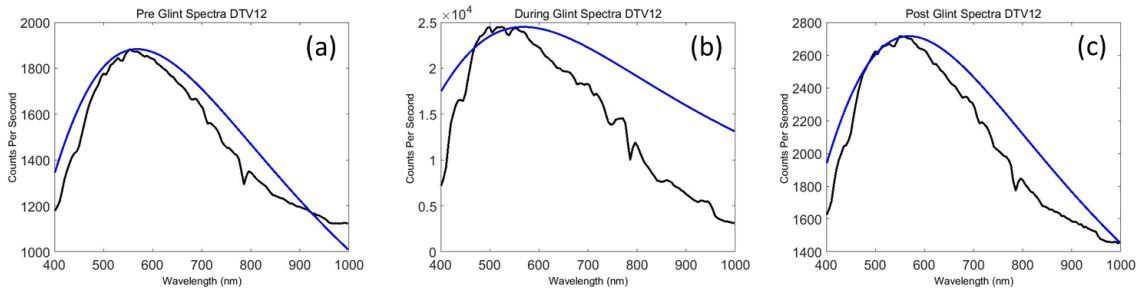

Fig. 20. DirecTV-12 average spectra (a) pre-glint, (b) during glint, and (c) post-glint. The blue trace indicates blackbody reflectance spectrum for a 4,987K object and the black trace indicates the data.

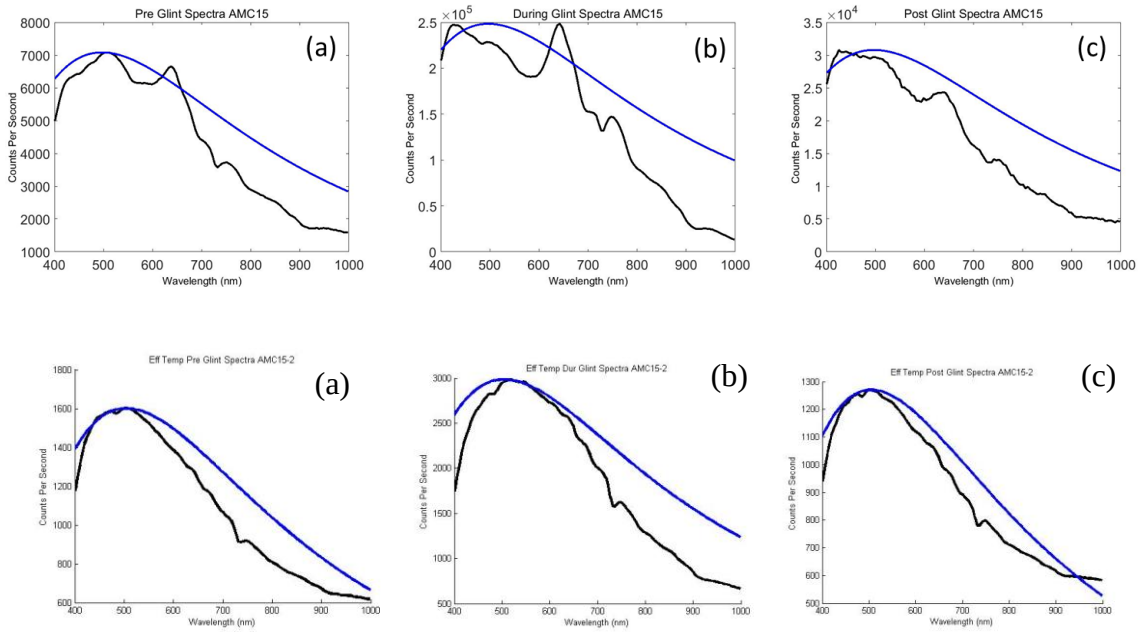

Fig. 21. AMC-15 average spectra (a) pre-glint, (b) during glint, and (c) post-glint as observed on 9 October 2015. The top row is from the first observation, and the second row is from the second observation. The blue trace indicates blackbody reflectance spectrum for a 5,786K object and the black trace indicates the data.

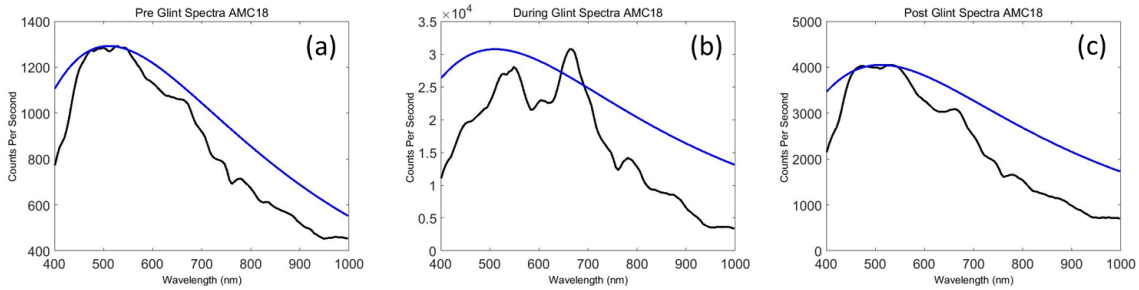

Fig. 22. AMC-18 average spectra (a) pre-glint, (b) during glint, and (c) post-glint. The blue trace indicates blackbody reflectance spectrum for a 5,711K object and the black trace indicates the data.

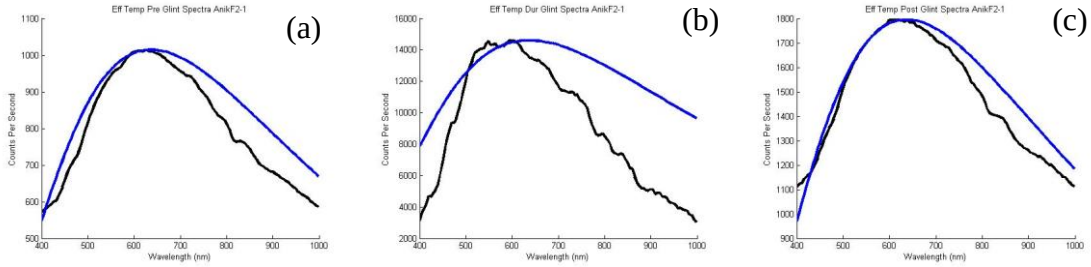

Fig. 23. AnikF2 average spectra (a) pre-glint, (b) during glint, and (c) post-glint. The blue trace indicates blackbody reflectance spectrum for a 4,526K object and the black trace indicates the data.

The corresponding blackbody curves are shown as the blue trace for temperatures represented by the satellite reflectance spectra before and after the glint, which are the same order of magnitude as the effective solar temperature of 5772K. Note that in order to visually compare the spectra, the individual y-axis range are different and the associated blackbody curves are scaled to match the maximum in the satellite spectra.

As one can see from Figs. 18-23, to first order, the average satellite spectra, with the possible exception of AMC-15 and AMC-18, before and after the glint appear to be more like a blackbody than during the glint. The satellite spectra during the glint are clearly not blackbody as a good portion of the solar spectrum greater than 600 nm is not reflected. This indicates that the surface causing the glint reflects primarily in the blue and is absorbing photons in the red, consistent with the characteristics of the typical older satellite solar panels. We offer these results as the definitive evidence that the source of a satellite's main glint during the equinox period is the specular reflection off the satellite's solar panels, a result that supports previous conclusions [9, 11].

For a quantitative analysis, we calculated the absolute differences between the glint spectra and blackbody curves or solar spectra for each satellite before, during, and after glint. Two different temperatures were used for the blackbody curves; effective satellite temperature and the temperature of the surface of the sun (5772K). Three different solar spectra were used for comparison; Extraterrestrial Radiation (ETR) [15], Direct and Circumsolar (Direct+), and Global Tilt [16]. ETR is the solar spectrum as observed from the top of the atmosphere at the mean Earth-Sun distance. Direct+ is the direct normal irradiance, or the radiation on the surface normal to the sun, excluding scattered sky and reflected ground radiation, plus circumsolar spectral irradiance, which excludes the radiation from the solar disk. Global Tilt is the spectral radiation form the solar disk plus sky diffuse and diffuse reflected from the ground, as measured from the ground on a south facing surface tilted 37 degrees from horizontal.

Absolute differences are reported as percentages of sun-effective-temperature blackbody in Fig. 24. It is clear that the glint spectra of the satellites have a 10-20% absolute difference relative to a blackbody (called a GS-BB Delta) when compared to the pre- and post-glint satellite spectra. The exception is AMC-15 which shows a GS-BB Delta that looks similar to the pre-glint spectral difference. This perhaps might be an indicator that the source of the AMC-15 glint is something other than the solar panels. However, if you compare Fig. 24 to Table 1, DirecTV-10/12 and Wildblue-1 have the larger percent difference and higher publicized power capacity compared to AMC-15/18.

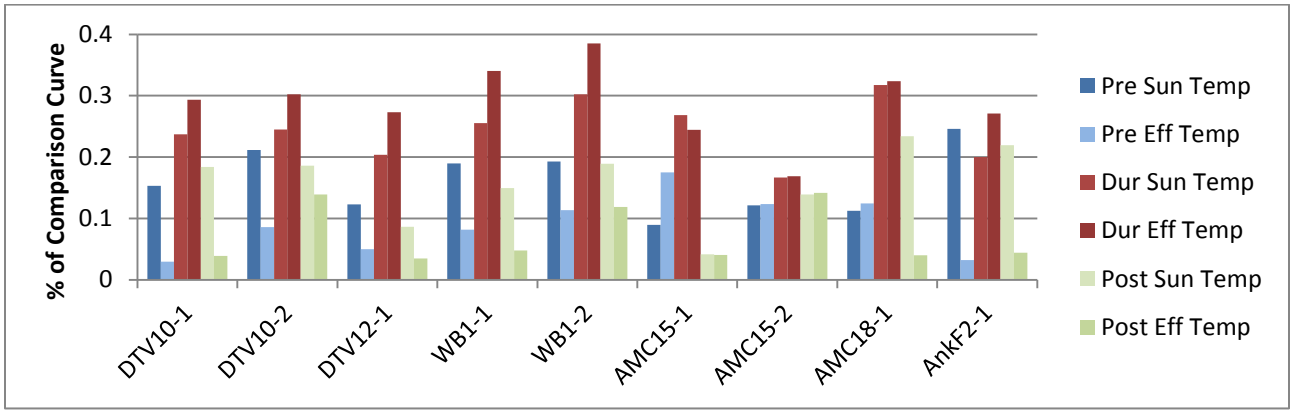

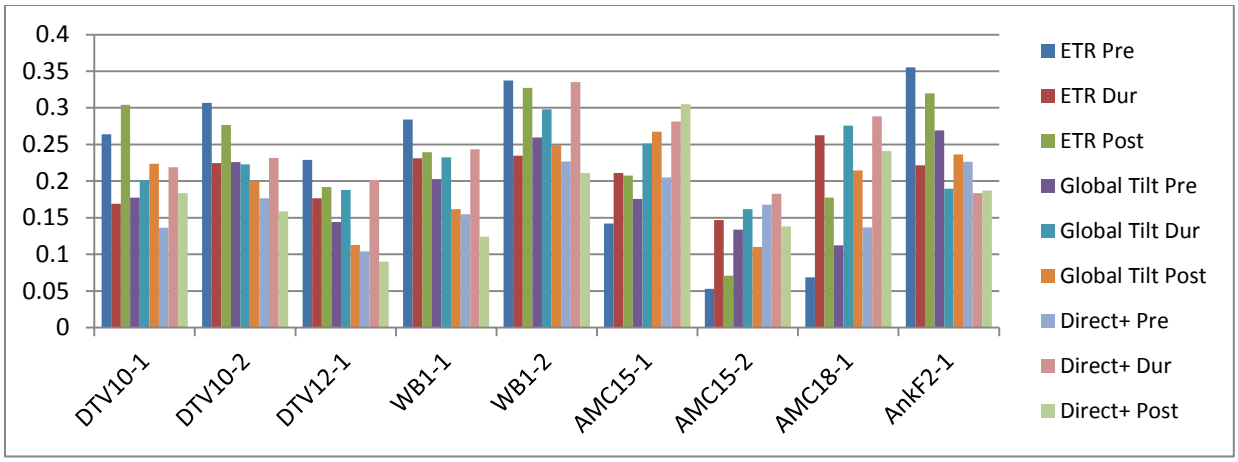

Fig. 24. Absolute Differences between glint spectra and blackbody curves. Pre, Dur, and Post refer to before-glint, during-glint, and after-glint, respectively.

These data were used to draw correlations between different metrics and satellite power. For each comparison technique, the average difference was taken between during and pre/post spectra differences. This gave an estimated change from in and out of glint for each comparison method. The standard deviation from the effective-temperature blackbody curve was taken to gauge on average how much the glint spectra differed from a blackbody at each wavelength interval, as opposed to total difference as measured with the other techniques. The differences of the standard deviations in and out of glint were also investigated. Satellite power was also compared to effective satellite temperature, as calculated from initial spectra data. All of these data were fitted with a linear function. The two best correlations are shown in Figures 25 and 26. This preliminary analysis shows that more data is needed before any meaningful correlation can be drawn, and more accurate satellite power data is needed to draw conclusive results.

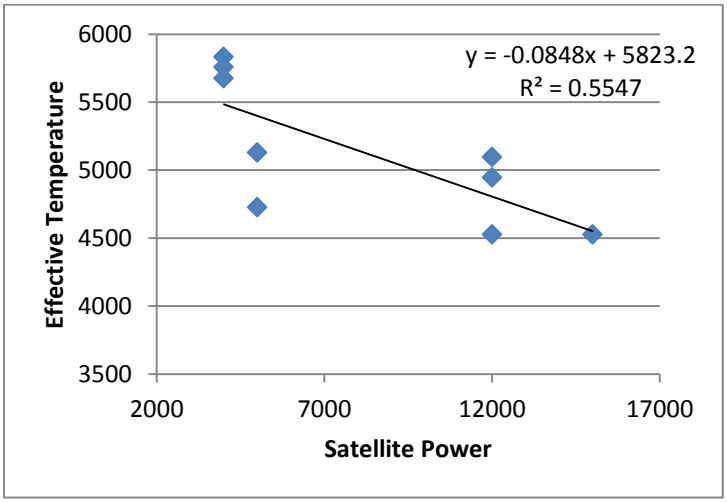

Figure 25. Correlation between satellite power and effective temperature. These data were fit with a linear function, shown in the upper right corner, with $R^2 = 0.5547$

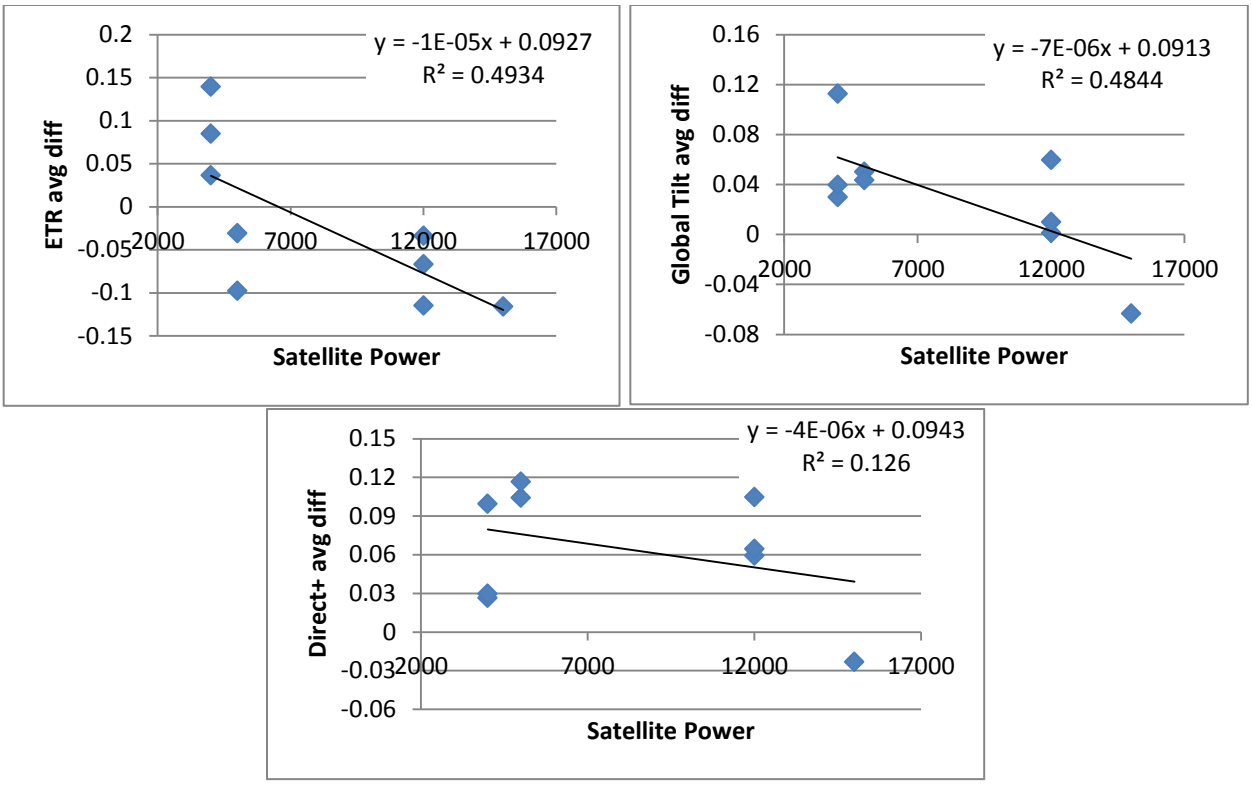

Figure 26. Correlations between satellite power and solar spectrum comparison data. These data were fit with linear functions, shown in the upper right corners

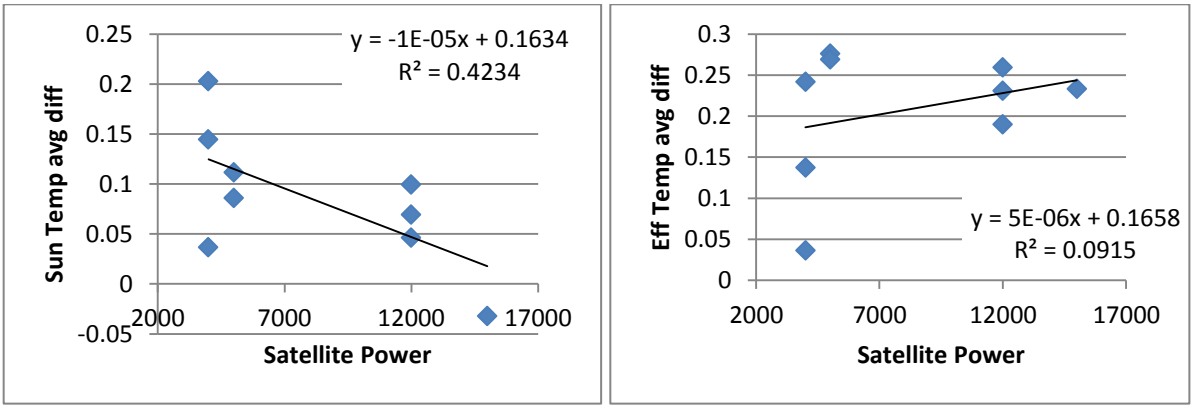

Figure 27. Correlations between satellite power and blackbody comparison data. These data were fit with linear functions, shown in the upper and lower right corners, respectively

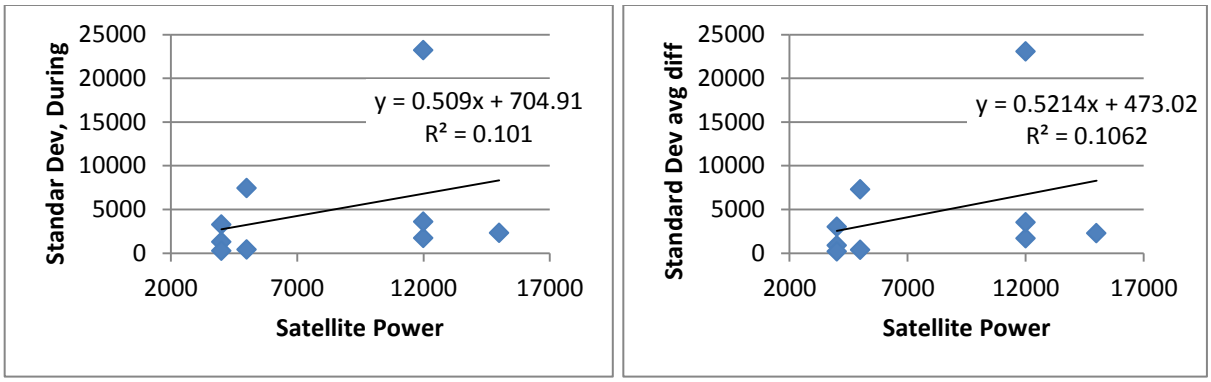

Figure 28. Correlations between satellite power and standard deviation data. The figure on the left shows standard deviation during glint, and the figure on the right shows the differences of the standard deviations between in and out of glint. These data were fit with linear functions, shown on the right

6. CONCLUSIONS

We demonstrate that slitless spectroscopy techniques can be used to discern characteristics of satellites. The full spectrum we collected on several satellites showed a very clear shift in spectral peak intensity from >550 nm outside of a glint to ~500 nm during glints. Additionally, although the satellite spectra before and after the glint appear to be blackbody-like, many of the satellite spectra during a glint do not, indicating that the glint is caused by a photon-absorbing satellite surface. These results support the contention that the primary source of most stabilized GEO satellite's glints is the solar panels. Further, a first-order quantitative analysis of the absolute difference between the satellite spectra before, during, and after a glint appear to show that the larger capacity solar panel systems have the largest absolute percent difference. More glint spectra measurements are clearly warranted, as well as improvements to our quantitative analysis.

7. ACKNOWLEDGEMENTS

The authors would like to thank the Air Force Office of Scientific Research whose funding supported this research.

8. REFERENCES

1 Payne, T. E., Gregory, S. A., Houtkooper, N. M., and Burdullis, T. W., "Classification of Geosynchronous Satellites Using Photometric Techniques", *Proceedings of the 2002 AMOS Technical Conference*, The Maui Economic Development Board, Inc., Kihei, Maui, HI, 2002.

2 Jorgensen, K., Okada, J., Africano, J., Hall, D., Guyote, M., Hamada, K., Stansbery, G., Barker, E., and Kervin, P., "Reflectance Spectra of Human-Made Space Objects," *The 2004 AMOS Technical Conference Proceedings*, The Maui Economic Development Board, Inc., Kihei, Maui, HI, 2004.

3 Hall, D., Calef, B., Knox, K., Bolden, M., and Kervin, P., "Separating Attitude and Shape Effects for Non-resolved Objects," *The 2007 AMOS Technical Conference Proceedings*, The Maui Economic Development Board, Inc., Kihei, Maui, HI, 2007.

4 Schildknecht, T., Vananti, A., Krag, H., and Erd, C., "Reflectance spectra of space debris in GEO," *The 2009 AMOS Technical Conference Proceedings*, The Maui Economic Development Board, Inc., Kihei, Maui, HI, 2009.

5 Bédard, D., Wade, G., Monin, D., and Scott, R., "Spectrometric characterization of geostationary satellites," *Proceedings of the 2012 AMOS Technical Conference*, The Maui Economic Development Board, Inc., Kihei, Maui, HI, 2012.

6 Lambert, J. V., "Measurement of the Visible Reflectance Spectra of Orbiting Satellites," *M.S. Thesis*, Air Force Institute of Technology, Dayton, OH, March 1971.

7 Hoag A. and Schroeder, D., "Nonobjective grating spectroscopy", *Publications of the Astronomical Society of the Pacific*, Vol. 82, No. 489 (October 1970), pp. 1141-1145.

8 Tippets, R. D., Wakefield, S., Young, S., Ferguson, I., Earp-Pitkins, C., and Chun, F. K., "Slitless spectroscopy of geosynchronous satellites," *Opt. Eng*. 54(10), 104103 (2015). doi: 10.1117/1.OE.54.10.104103.
9 Payne, T. E., Gregory, S. A., and Luu, K., "SSA Analysis of GEOS Photometric Signature Classifications and Solar Panel Offsets," *Proceedings of the 2006 AMOS Technical Conference*, The Maui Economic Development Board, Inc., Kihei, Maui, HI, 2006.
10 Dunsmore, A.N., J.A. Key, R.M. Tucker, E.M. Weld, F.K. Chun, and R.D. Tippets, "Spectral Measurements of Geosynchronous Satellites During Glint Season," *accepted by J. of Spacecraft and Rockets*, 2016.
11 Vrba, F. J., DiVittorio, M. E., Hindsley, R. B., Schmitt, H. R., Armstrong, J. T., Shankland, P. D., Hutter, D. J., and Benson, J. A., "A survey of geosynchronous satellite glints." *The 2009 AMOS Technical Conference Proceedings*, The Maui Economic Development Board, Inc., Kihei, Maui, HI, 2009.
12 Cook, R.L and Torrance, K.E., "A Reflectance Model for Computer Graphics", *ACM Transactions on Graphics*, Vol.1, 7-24, 1982.
13 West, D., "Resolution Calculation for a Slitless Spectrograph," URL: http://users.erols.com/njastro/faas/articles/west01.htm [cited 2 September 2015].
14 Hall, D., Hamada, K., Kelecy, T., and Kervin, P., "Surface Material Characterization from Non-resolved Multi-band Optical Observations," *The 2012 AMOS Technical Conference Proceedings*, The Maui Economic Development Board, Inc., Kihei, Maui, HI, 2012.
15 URL: http://rredc.nrel.gov/solar/spectra/am0/am0_index.html#spectrum [cited 23 August 2017].
16 URL: http://rredc.nrel.gov/solar/spectra/am1.5/ [cited 23 August 2017].